AAPS PharmSciTech (2024) 25:214
https://doi.org/10.1208/s12249-024-02932-5

RESEARCH ARTICLE

Exploring Co-Amorphous Formulations Of Nevirapine: Insights From Computational, Thermal, And Solubility Analyses

Kayque Almeida dos Santos[1] · Luíse Lopes Chaves[1,2] · Daniela Nadvorny[2] · Mônica Felts de La Roca Soares[1,2] · José Lamartine Soares Sobrinho[1]

Received: 20 June 2024 / Accepted: 3 September 2024

Abstract

This study aimed to assess the formation of nevirapine (NVP) co-amorphs systems (CAM) with different co-formers (lamivudine—3TC, citric acid—CAc, and urea) through combined screening techniques as computational and thermal studies, solubility studies; in addition to develop and characterize suitable NVP-CAM. NVP-CAM were obtained using the quench-cooling method, and characterized by differential scanning calorimetry (DSC), X-ray diffractometry (XRD), Fourier Transform Infrared Spectroscopy (FTIR), and polarized light microscopy (PLM), in addition to *in vitro* dissolution in pH 6.8. The screening results indicated intermolecular interactions occurring between NVP and 3TC; NVP and CAc, where shifts in the melting temperature of NVP were verified. The presence of CAc impacted the NVP equilibrium solubility, due to hydrogen bonds. DSC thermograms evidenced the reduction and shifting of the endothermic peaks of NVP in the presence of its co-formers, suggesting partial miscibility of the compounds. Amorphization was proven by XRD and PLM assays. *In vitro* dissolution study exhibited a significant increase in solubility and dissolution efficiency of NVP-CAM compared to free NVP. Combined use of screening studies was useful for the development of stable and amorphous NVP-CAM, with increased NVP solubility, making CAM promising systems for combined antiretroviral therapy.

Keywords biopharmaceutical classification system (BCS) · co-amorphous · HIV · solubility

Introduction

HIV infection still represents a public health problem, having caused more than 40 million deaths around the world to date, with continuous transmission in every country in the world [1]. Although there is no cure for the infection, the use of a combination therapy comprising three or more anti-HIV drugs, called highly active antiretroviral therapy (HAART), was a major advance in controlling HIV infection and preventing the progression of the disease. On the other hand, the daily need for multiple tablets in addition to the potential for significant side effects still constitutes a therapeutic challenge. Additionally, most of the more than 25 FDA-approved anti-HIV drugs administered orally have poor water solubility, limiting the rate and extent of drug absorption [2].

Among the drugs used in HAART, nevirapine (NVP) is one of the drugs used in pediatric therapeutic regimens, specifically for neonates and infants, to prevent mother-to-child vertical transmission, in association with other anti-HIV drugs, with zidovudine and lamivudine, which chemical name is 2',3'-dideoxy-3'-Thiacytidine (3TC) [3]. Despite its notable importance in HAART, NVP is classified as class II according to the biopharmaceutical classification system (BCS), directly impacting the absorption of the drug, since its molecules need to be dissolved in the fluids of the gastrointestinal tract, which are aqueous solutions [4, 5].

Therefore, class II drugs have slow absorption that leads to gastrointestinal mucosal toxicity and inadequate and variable bioavailability, which, to be mitigated, requires higher doses to obtain therapeutic benefits that can lead to adverse effects on the patient and negatively affect patient adherence to treatment [6, 7]. As a result, the improvement in drug

✉ José Lamartine Soares Sobrinho
joselamartine@hotmail.com

[1] Quality Control Core of Medicines and Correlates – NCQMC, Department of Pharmaceutical Sciences, Federal University of Pernambuco, Recife, PE, Brazil

[2] Postgraduate Program in Pharmaceutical Sciences, Pharmaceutical Sciences Institute, Federal University of Alagoas, Maceió, Alagoas, Brazil

Published online: 12 September 2024

solubility is the focus of continued efforts in the bio/pharmaceutical drug development sector [3]. Therefore, several technologies have been applied with the aim of increasing the solubility of drugs as solid dispersions [3, 8], nanoparticles [9], nanosuspensions [10], and self-emulsifying drug delivery systems [11, 12], besides the use of chemicals as surfactants [13], cyclodextrins [14].

In this context, supersaturated amorphous systems have proven to be an excellent strategy to improve the absorption of drugs with low aqueous solubility as supersaturation drives rapid and sustained absorption in the gastrointestinal tract after dissolution [15]. This solubility improvement may result in enhanced bioavailability, a reduction in the required dosage, and a potential decrease in adverse effects, thereby increasing the overall efficacy and patient compliance in clinical settings. However, materials in the amorphous form have excess energies, like free Gibbs energy, enthalpy, and entropy, promoting an increase in aqueous solubility and dissolution rates [16, 17]. Nevertheless, the elevated energy state results in recrystallization, which converts the amorphous material to its crystalline counterpart. This process entails the loss of the solubility advantage associated with the amorphous form [18].

The use of polymeric carriers as an additional component has been used to stabilize the amorphous molecule in a drug delivery system named amorphous solid dispersions, avoiding drug recrystallization and promoting its supersaturation above their equilibrium solubility when in solution in the gastrointestinal tract, elevating [19] the other hand, the large quantity of polymers required to maintain supersaturation, associated with the high hygroscopicity of most polymers used for this purpose, makes the use of these systems limited, especially in pharmaceutical forms of drugs with high dosages [20].

Alternatively, the application of small molecules has emerged as an alternative to polymers, forming a homogeneous amorphous phase with the drug through intermolecular interactions, creating a new drug delivery system known as co-amorphous (CAM) [21–23]. This approach has some potential advantages over ASD and simple amorphous materials as the drug load can be increased from 20–30 wt % to approximately 50 wt % or even higher in many cases, increasing the stability of CAM systems compared to the amorphous solids while retaining the dissolution advantage of an amorphous form [22].

The low-molecular-weight coformers may be other drug substances or low-molecular-weight excipients such as amino acids, organic acids, and other small molecules, such as urea (URE) and citric acid (CAc). The coformer physically stabilizes the amorphous form of the drug either by interacting with the drug on a molecular level (e.g., by salt formation, hydrogen bonding, and pi–pi interactions) or simply by molecular mixing [24]. The miscibility of the drug and coformer is one of the main issues for the successful formation of a CAM, and this parameter can be determined by experimental, theoretical, and/or computational approaches [22]. The use of a second drug as a coformer presents additional advantages when compared to other small molecules as they can serve as platforms to achieve potential combined therapies, being able to increase efficacy, reducing toxicity and side effects to a large extent, in addition to presenting economic benefits [25, 26]. In this context, this study aimed to develop CAM systems to increase the aqueous solubility of NVP, performing screening of possible coformers molecules among other drugs and excipients.

Material and Methods

Material

NVP was purchased from Farmanguinhos (Rio de Janeiro, Brazil). 3TC was donated by the Pharmaceutical Laboratory of Pernambuco (LAFEPE). CAc and URE were purchased from Neon®. Ultrapure water was obtained using the MilliQ® system (Milipore, Bedford, USA). All other reagents and solvents were of analytical grade or liquid chromatography grade and were purchased and used as soon as received.

Screening of CAM formation

Screening of Coformers

The selection of suitable coformers to stabilize the amorphous form of a drug tends to be conducted on a case-by-case basis. Therefore, the selection of the coformers was based on their chemical information, mainly on the number of H^+ donors and acceptors, since the presence of donor and acceptor groups can generate hydrogen interactions between the molecules [27]. The melting point was verified due to the use of temperature for the development of CAMs. Compounds chemical information has been given in Supplementary File 1.

Computational Studies

The Software *Gaussview* (Gaussian, Inc.) was used to construct the molecular structures of NVP, 3TC, CAc, urea, and hydrogen complexes [28]. The obtained structures were used to generate electrostatic potential maps, which illustrate the three-dimensional charge distributions of the molecules on their surfaces, where red represents the most electronegative region and blue highlights the most electropositive, enabling interpretations regarding the possibilities of formation of sites of interaction between the drug and coformer. Calculations were performed using the Gaussian 09 computational package to perform geometry and harmonic

frequency optimization through the HF/3-21G calculation level [29]. Through calculations, the values of the intermolecular hydrogen bond energy were found (the more negative the energy, the more stable the hydrogen interaction).

Thermal Analysis DSC

A DSC equipment (8000 model PerkinElmer; PyrisTM Player software) was used to verify the miscibility between the components and the tendency to generate amorphous systems using controlled heating and cooling rates, and characterizing the product obtained as reported by D'Angelo et al. [30]. Briefly, 3 mg (±0.5 mg) of crystalline NVP and its physical mixtures samples with the coformers in 1:1 molar ratio were added into a hermetically sealed aluminum pan. The heating and cooling program is described in Table I. Initially, the samples were equilibrated at 0 °C and heated to a temperature that was above the lowest melting point of the component present in each sample, at a heating rate of 20 °C/min, whose balance was maintained for 2 min. They were then cooled to 0 °C at a cooling rate of 20 °C/min and reheated to 300 °C at 10 °C/min since NVP degrades after this temperature [31]. Indium metal standard with purity of 99.9% was used to calibrate the temperature scale and enthalpy response.

Determination of Equilibrium Solubility

The crystalline solubility of NVP was determined by the shake flask method in phosphate buffer pH 6.8 methods [32, 33]. Erlenmeyer flasks with 10 ml of buffer were saturated with an excess amount of crystalline NVP in the absence and presence of each coformer and maintained at 37 °C and shaken at 150 rpm in an orbital incubator (Ethik Technology, São Paulo, BR) for 3 days with the intention of verifying the influence of coformers on the equilibrium solubility of NVP. The collected samples were centrifuged at 14,000 rpm for 5 min, the supernatant was removed and diluted for quantification by liquid chromatography (Shimadzu®) according to the methodology described in the section Analytical Chromatographic conditions.

Obtention of Physical Mixtures and CAM

The CAM with NVP were obtained according to the methodology proposed by Skotnicki *et al*. [34]. Samples of NVP and coformers were carefully weighed in a 1:1 molar ratio, and ground with a mortar and pestle to promote intimate contact and obtain physical mixtures (PM). The CAM were obtained by melting their respective PMs in a steel container on a heating plate at 260 °C. After the phase change, the container was quickly taken to an ice bath for immediate cooling. The resulting powder was crushed, standardized to a size of 150 µm, and stored in a desiccator with silica.

Table I Heating/Cooling/Reheating Program in DSC for Physical Mixtures of NVP and Coformers Screened to Obtain CAM

Sample	Program
NVP	0 °C—260 °C—25 °C—300 °C
NVP-3TC	0 °C—165 °C—25 °C—300 °C
NVP-CAc	0 °C—160 °C—25 °C—300 °C
NVP-URE	0 °C—260 °C—25 °C—300 °C

Solid State Characterization

Fourier Transform Infrared Spectroscopy (FTIR)

FTIR spectra of the pure samples, PM and CAMs were obtained on a PerkinElmer® equipment (model 400) with a total reflection device attenuated with zinc selenide crystal. The spectra were obtained in transmittance mode by averaging 16 scans per sample, with a variation in the wavenumber region 4000 to 650 cm^{-1}.

Differential Scanning Calorimetry (DSC)

The DSC curves of the pure compounds, PM and CAM were obtained using a Shimadzu® DSC equipment, model DSC-50, connected to the Shimadzu® TA-60WS software with a nitrogen atmosphere (50 ml/min) in the temperature range of 25–300 °C at a rate of 10 °C/min. Sample amounts of 3–4 mg were placed in hermetically sealed aluminum pans. Indium standard with purity of 99.9% was used to calibrate the temperature scale.

X-Ray Diffractometry (XRD)

X-ray diffractometry analyses were carried out using a Shimadzu diffractometer, X-ray—7000, using X-rays generated by a Cu (Kα) anode, operated at 40 kV voltage, 30 mA current and Ni filter. An angular variation (2θ) of 3- 60° was used, with a continuous scanning speed of 2°/min. For the quantification of the crystalline content in the PMs and CAMs, the integrated areas of the NVP diffraction peaks and coformers in the analyzed samples were calculated by curve fitting using software (Origin 2018, OriginLab Co, Northampton, MA, EUA).

Polarized Light Microscopy (PLM)

Microscopic analyses were performed on a Leica DM750M polarized light microscope, coupled with a digital camera (Leica ICC50W) and processed in the LAS EZ software. Lesser amounts of the powdered samples were placed on semi-permanent glass slides and analyzed using 200× magnification (Olympus Corporation, Tokyo, Japan).

Analytical Chromatographic conditions

Quantification of NVP was carried out in an HPLC equipment composed of Shimadzu's 10AVP series system, equipped with an LC-10AVP quaternary pump, an SPP-M10AVP ultraviolet detector according to an adapted method of Vieira-Sellaï *et al*. [35] and Anbazhagan *et al*. [36]. Data acquisition was performed using LC Solutions software (version 1.25). Chromatographic separation occurred on a C8 Shim-Pack column (150 × 4.6 mm; 5 µm), at a temperature of 25 °C and injection volume of 10 µm. Separation was achieved in low pressure gradient mode using 25mM ammonium acetate buffer pH 3.9 as mobile phase A, and methanol as mobile phase B. The gradient profile (%v/v) consisted of a linear increase in phase B from 25 to 75% within 7 min while A decreased linearly from 75 to 25% at the same time. The phase proportion inverted between 7 and 8 min and remained isocratic until the end of the analysis, in 15 min. The calibration curve demonstrated good linearity ($R > 0.99$) in the relevant concentration range and a preliminary analysis performed showed that 3TC, CAc and URE do not interfere with the retention time of NVP (10.5 min).

In Vitro Dissolution Test

The dissolution test was evaluated in sink condition in a Vankel VK-7040 Dissolutor according to the methodology proposed by Santos *et al*. [3]. Samples of pure NVP (20 mg) and the equivalent in drug of PM and CAM were weighed and placed in 250 mL in phosphate buffer pH 6.8 at 37 ± 0.5 °C stirred by the paddle apparatus at 75 rpm. Samples were collected at predetermined times (5, 10, 15, 20, 30, 45, 60, 90, 120, 180, 240, 300, and 360 min), centrifuged and the supernatant was quantified by HPLC, using the method described before. The dissolution profiles of all samples were evaluated for dissolution efficiency (DE%) at 120 min and 360 min (DE% 120 and 360) and similarity factor (F2) using the DD SolverTM software [37, 38].

Statistical Analysis

One-way analysis of variance (ANOVA) and Tukey's multiple comparison tests were performed to verify the statistical significance ($p < 0.05$, 95% confidence interval) of the comparisons between the pure NVP, PMs and CAMs.

Results

Screening of CAM Formation

Computational Studies

NVP map evidenced an electronegative region with high density in its carbonyl (-C = O) of the central aromatic ring, as well as an electropositive region referring to the amine (Fig. 1), while 3TC has a carbonyl on the aromatic and hydroxyl ring, forming two complexes together (Fig. 2a and b). The energy resulting from the formation of hydrogen bonds for complexes NVP-3TC A and B were -8.96 and -14.42 kcal/mol, respectively. The hydroxyl regions of CAc were characterized by electropositive bands located throughout all molecular structure (Fig. 2c). These regions can interact with NVP, forming two complex structures from the simultaneous interaction of its carbonyls and hydroxyls from the central part or molecular end, with the carbonyl and amino group of NVP (Fig. 2c and d), which have remarkably close hydrogen bond energies, -23.74 and -22.83 kcal/mol for structures C and D respectively, resulting in greater stability to the formed system.

A theoretical infrared spectrophotometric analysis was performed (Fig. 3) showing changes in the vibrations of the groups responsible for hydrogen interactions in the molecules of the complexed compounds. NVP has a stretch band of its carbonyl at 1880 cm^{-1} that was shifted to 1840 cm^{-1} and 1854 cm^{-1} in the 3TC complexes 1 and 2, which also showed the emergence of new bands at 3703 cm^{-1} and 3559 cm^{-1} respectively, which may indicate the formation of hydrogen complexes through the -NH an -OH groups present in the two compounds. Furthermore, interactions between -OH and –NH bonds involved in the formation of the CAc complexes also are also suggested by the appearance of high intensity bands in 3532 cm^{-1} and 3010 cm^{-1} in the CAc complex 1 and 3505 cm^{-1} and 3136 cm^{-1} in the CAc complex 2. In the two CAc complexes, the stretch band of the carbonyl = O of NVP was also shifted to 1867 cm^{-1} and 1858 cm^{-1}, suggesting intermolecular interactions in the two complexes between NVP and CAc. No bond formations were observed between NVP and URE molecules.

Thermal Analysis by DSC

DSC curves and thermic data are shown in Fig. 4 and Supplementary File SII respectively. Pure NVP presented its characteristic melting point at 248°C, and an exothermic

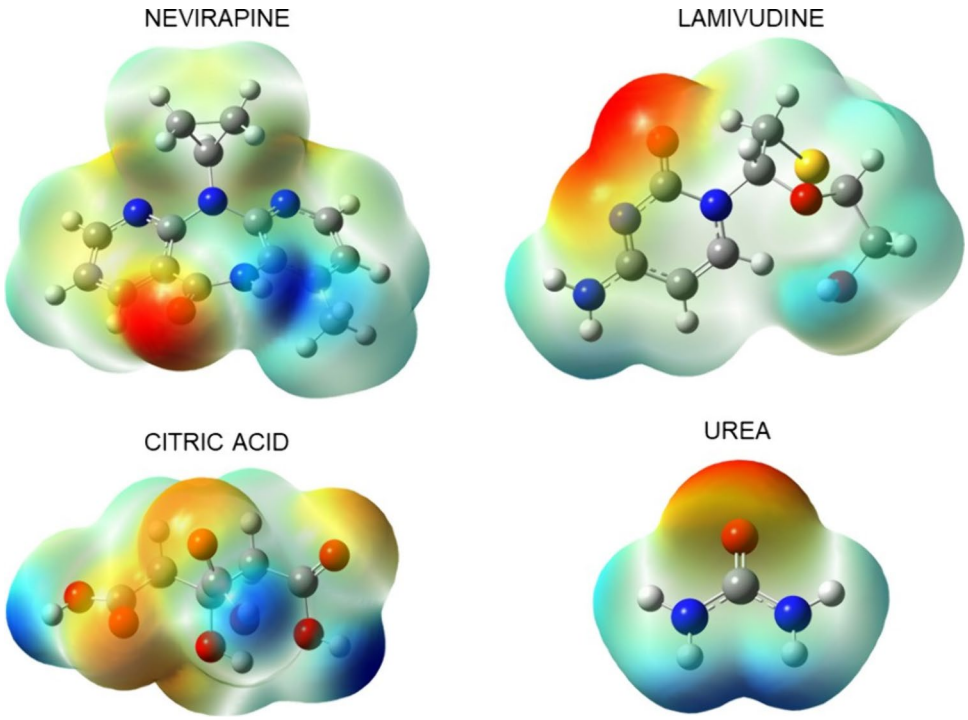

Fig. 1 Electrostatic potential maps of NVP, 3TC, CAc and URE. Regions in red represent electronegative sites and regions in blue represent electropositive sites

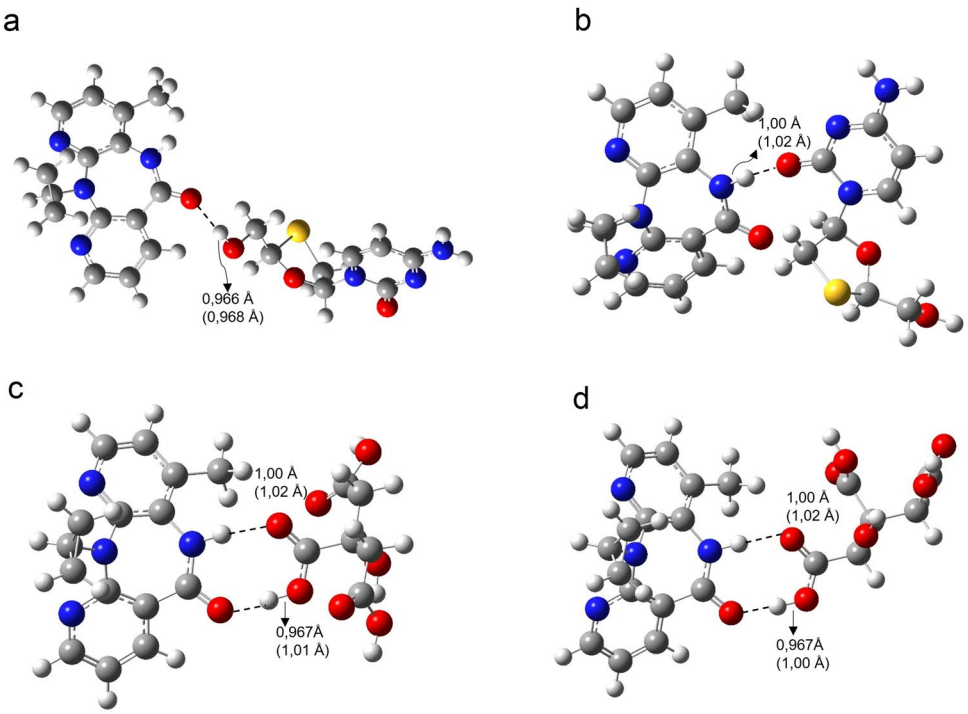

Fig. 2 Complexes formed between NVP, 3TC (**a** and **b**) and CAc (**c** and **d**) through the Gaussview v.05 program

band was also detected around 175°C. DSC curves of NVP-3TC PM and NVP-CAc PM showed the shift of NVP melting point at 235.2°C and 238.7°C respectively, with an endothermic peak in the mixture with 3TC at 175.1°C corresponding to the 3TC melting point [39]. The NVP-URE mixture presented an endothermic peak that indicates the melting point of NVP at 242.5°C.

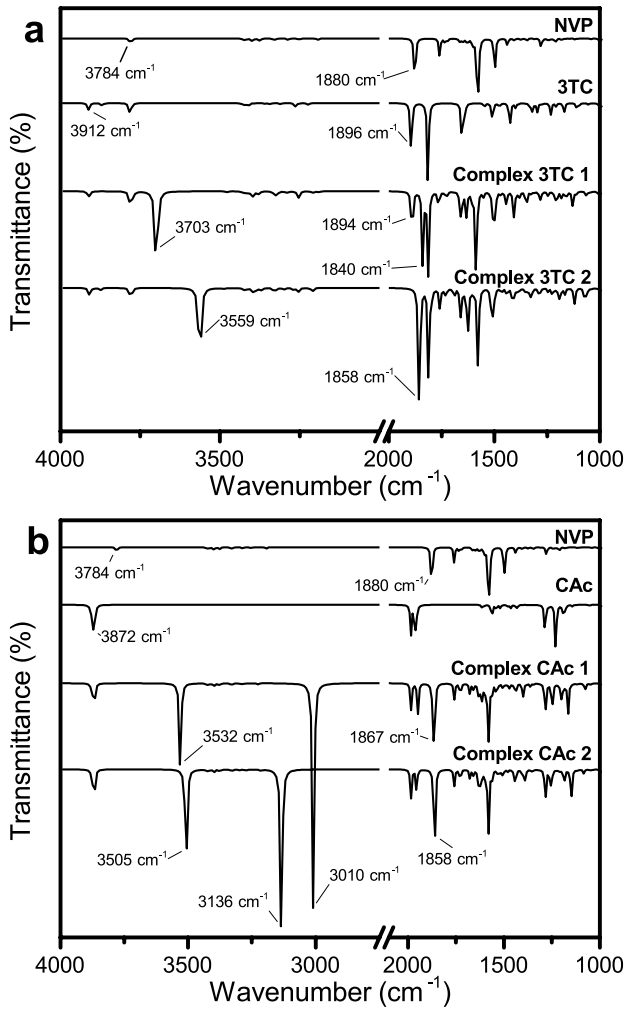

Fig. 3 Theoretical infrared spectrum of complexes formed between NVP with 3TC (**a**) and CAc (**b**)

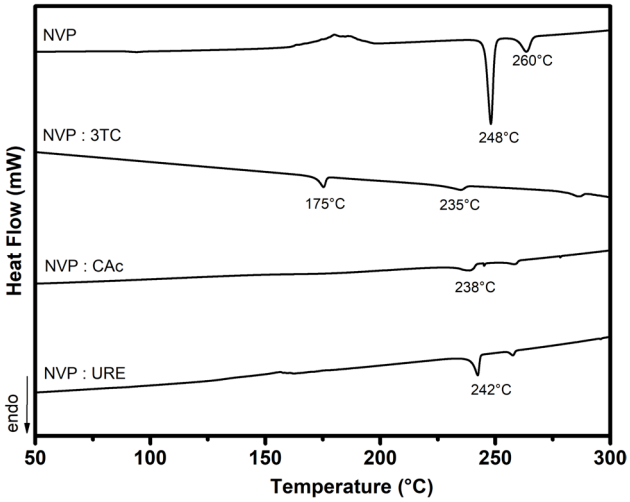

Fig. 4 DSC curves of NVP, NVP—3TC, NVP—CAc and NVP—URE during the second heating

Determination of Equilibrium Solubility

NVP concentration values for each sample analyzed are described in Supplementary File III. They are known as saturation concentration or equilibrium solubility. The maximum concentration achieved by NVP was approximately 104.6 µg/mL, being altered at the presence of 3TC, increasing NVP solubility to 114.9 µg/mL, as well as the CAc, which also raised the NVP concentration to 662.46 µg/mL. URE also was able to increase NVP solubility to 132.98 µg/mL.

Solid State Characterization

X-ray Diffractometry (XRD)

The diffractogram patterns of NVP, 3TC, and CAc, as well as their PM and CAMs are illustrated in Fig. 5. The diffraction planes indicating the crystalline nature of NVP were detected at 9.04°, 12.91°, 15.46°, 17.09°, 18.91°, 20.64°, 22.49°, 23.19°, 25.33° and 26.55°, following previous results reported in the literature [40, 41]. All PMs obtained showed the presence of NVP and the coformer used by their characteristic diffraction planes, while the absence of peaks was observed in the CAMs of 3TC and CAc.

Fourier Transform Infrared Spectroscopy (FTIR)

NVP groups are represented in the infrared spectrum (Fig. 6A) at 3188 cm^{-1} and 1642 cm^{-1} corresponding to the vibrational nodes of the stretching -NH and -C = O respectively of the amide group. The spectrum also shows bands at 3123 cm^{-1} that correspond to the -CH bond of the cyclopropyl substituent and at 1584 cm^{-1} that characterize the scissor vibrations of the -CH3 methyl group. The spectrum of 3TC is characterized by the presence of the carbonyl group (-C = O) vibration of the carbamide function at 1633 cm^{-1}, deformation of the -NH group at 1607 cm^{-1} and broad bands of stretching vibration of the -NH2 group at 3328–3500 cm^{-1} [39, 42]. Broadenings in the stretching bands at 3328 cm^{-1} of 3TC and at 3188 cm^{-1} of the -NH group of the NVP amide were evident in the CAM NVP:3TC, especially when compared to PM, with shift to the right of the stretching vibration band of the $-NH_2$ group of 3TC. CAc is identified by a -OH stretching vibration at 3492 cm^{-1} and at 3328 cm^{-1} of the carboxylic group (-COOH) [43, 44]. The two peaks at 1692 cm^{-1} and 1743 cm^{-1} in the FTIR spectra of CAc arise from the C = O stretch in the carboxylic groups. Both peaks overlap as they move across the NVP:CAc CAM spectrum, while still being present in the PM. Its hydroxyl stretching bands (-OH) had reduced and broadened intensities in the

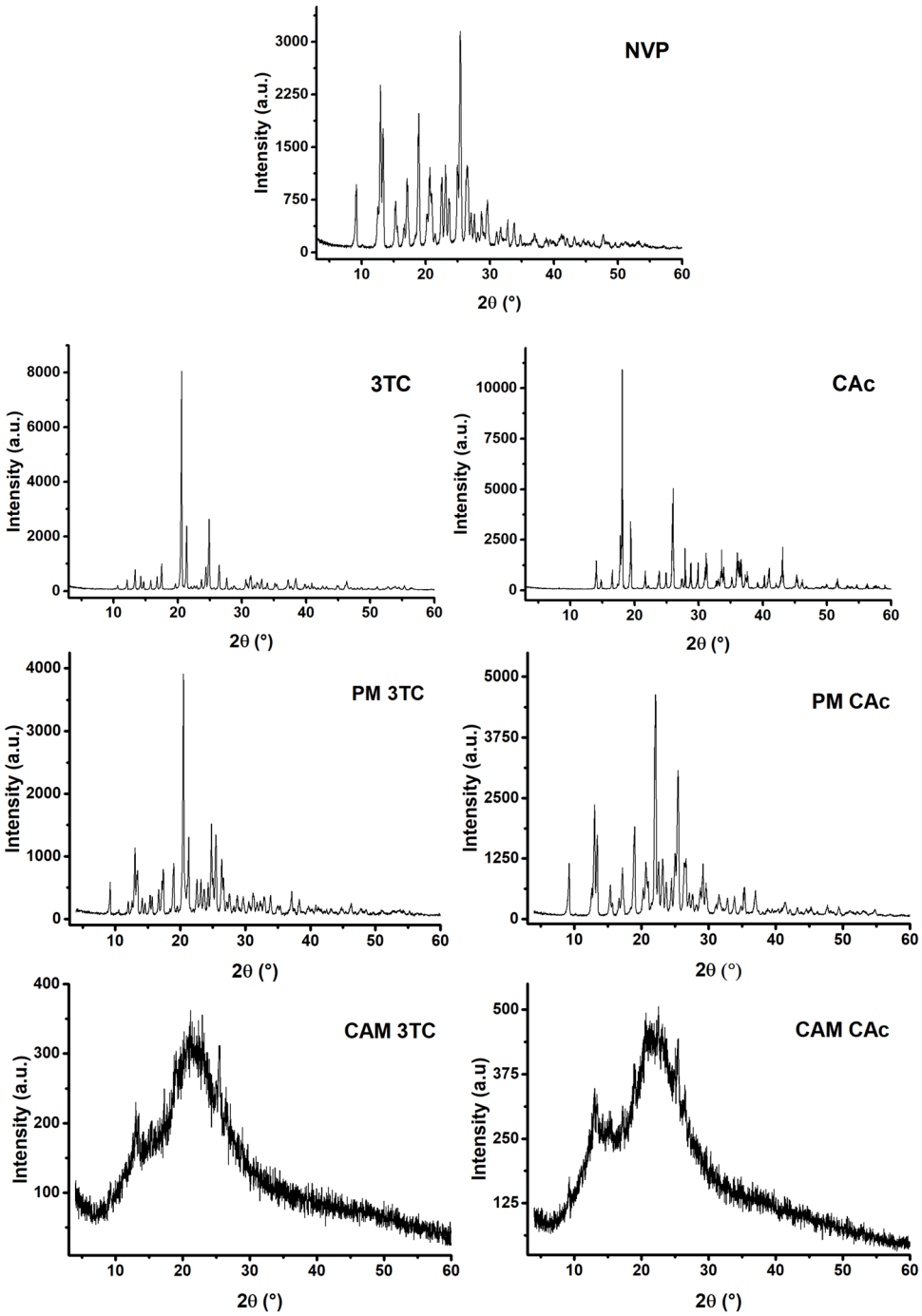

Fig. 5 X-ray diffraction patterns of NVP, 3TC and CAc, their respective PM and CAM

PM with NVP, in addition to the broadening of the C = O stretching in the CAM.

Differential Scanning Calorimetry (DSC)

DSC analysis were performed with the NVP pure, coformers, their PM and CAM (Fig. 7 and Supplementary File IV). NVP has a characteristic melting point at 244°C and 3TC at 175°C. In the PM 3TC, two endothermic fusion peaks were identified with a maximum peak at 175°C and another at 230°C, while in the CAM 3TC, only one endothermic band was identified at 230°C, with an exothermic band at around 135°C. In addition, a Tg was identified at 52°C in CAM 3TC, CAc has a melting peak at 154°C that appears shifted in PM CAc at 132°C, where an endothermic peak at 230°C was also revealed for NVP fusion. In CAM CAc, a Tg was detected at 63°C, followed by an exothermic recrystallization event at 133°C and an endothermic fusion peak referring to NVP at 239°C.

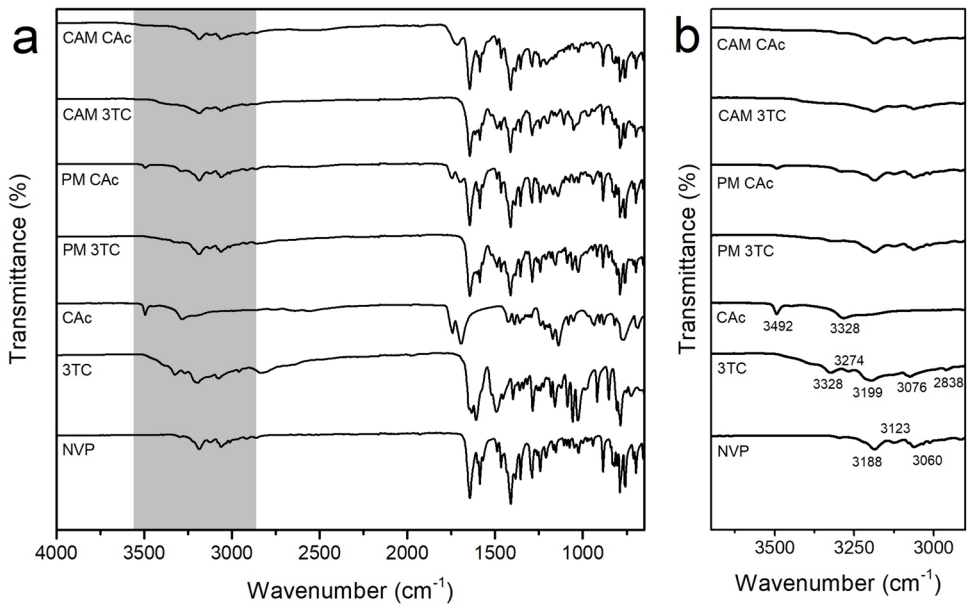

Fig. 6 FTIR spectrum with wavenumber from 4000 to 600 cm^{-1} (**a**) and with a cutoff in the region from 3560 to 2850 cm^{-1} (**b**) of NVP, 3TC, CAc, their PM and CAM

Polarized Light Microscopy (PLM)

PLM photographs were taken to observe the presence of microcrystals in the generated systems and are illustrated in Supplementary File V. NVP and 3TC are characterized by small colored dots on the photographs, indicating crystalline material, while CAc is represented by a huge mass with colored regions indicating the crystalline nature of the

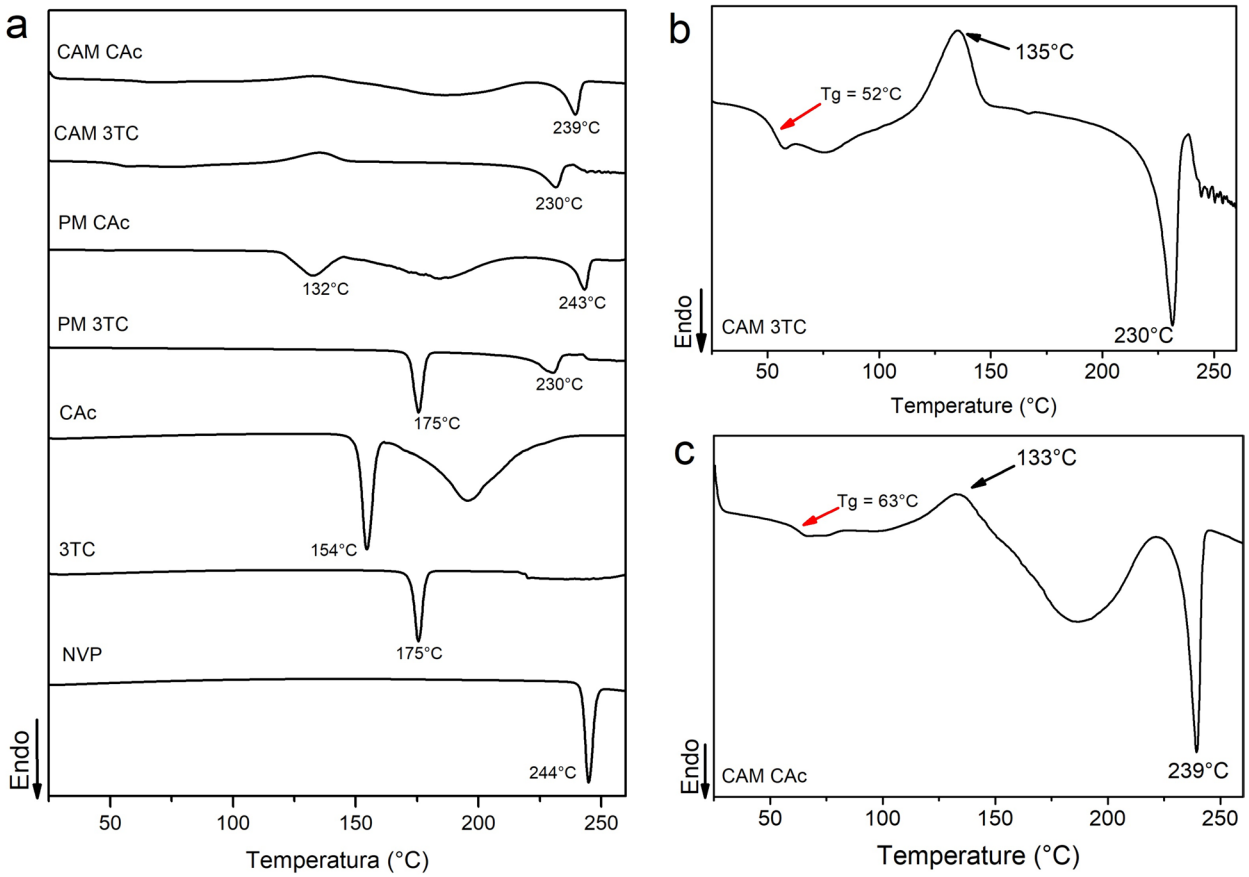

Fig. 7 DSC curves of pure components, PM and CAM (**a**), with magnification of the DSC curve of the CAM 3TC (**b**) and the CAM CAc (**c**)

excipient. Numerous crystalline points were noted on the slides of all PM, showing that the simple mixture between the components is not enough to promote the amorphization of the drug. However, the CAMs showed significant differences in relation to their respective mixtures, where no crystalline points with birefringence were visualized.

In Vitro Dissolution

The dissolution profiles of NVP pure, PMs and CAMs are illustrated at Fig. 8 and quantitative data of dissolution are shown in Table II and Supplementary File VI. After *in vitro* dissolution tests, it was observed that pure NVP achieved a dissolution of 64% at 360 min, while all CAMs reached higher levels of NVP dissolved, mainly CAM 3TC which had the highest dissolution rate (97.58%) followed by CAM CAc (93.88%). CAM 3TC had the highest dissolution efficiency, with values of 68.7% in 120 min and 81.7% in 360 min, also showing the difference between these samples with a similarity factor (F2) of 20.6 for pure NVP and 37.9 for its PM. CAM CAc showed excellent dissolution performance with 62.6% of NVP in 120 min and 62.9% in 360 min. Although it was not statistically different in relation to its PM at the final time, CAM CAc had an excellent dissolution performance, with a similarity factor (F2) of 23.6 for pure NVP and 55.8 for its PM, showing that there was a difference between the samples during the assay.

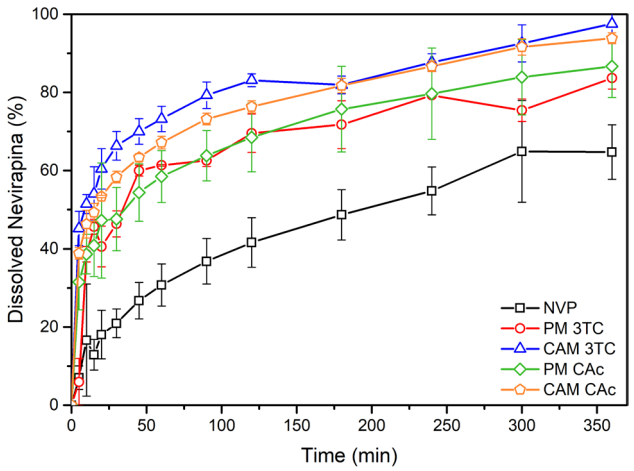

Fig. 8 NVP dissolution profiles with 3TC and its PM and CAM and CAc and its PM and CAM

Table II Dissolution Efficiency of NVP and its PM and CAM with 3TC and CAc at Times in 120 min and 360 min

Samples		Dissolution efficiency (%)	
		120 MIN	*360 MIN*
Pure NVP		28.2 ± 4.7	46.3 ± 6.6
NVP—3TC	*PM*	54.3[*a] ± 1.8	68.6[*a] ± 2.8
	CAM	68.7[*a,b] ± 2.3	81.7[*a,b] ± 2.1
NVP—CAc	*PM*	54.2[*a] ± 3.3	56.6[*a] ± 2.8
	CAM	62.6[*a,c] ± 1.3	62.9[*a] ± 0.6

Mean ± SD, $n = 3$;

[*]Statistically different $p < 0.05$ *vs.* [a]NVP, [b]PM 3TC e [c]PM CAc

Discussion

Suitable coformers are crucial for the development of a stable CAM. To achieve this, screening experiments are important to predict the interaction between the components, and thus, the possible formation of CAM using low molecular weight components, such as URE and CAc [45–49], in addition to 3TC, an antiretroviral drug used in multidrug therapy with NVP to combat HIV. Molecular and thermal analysis studies can provide information regarding the possible intermolecular interactions that can occur between NVP and its coformers, and which regions of the molecule have the greatest potential for these interactions, while solubility studies evaluate the impact that the presence of these substances has on the crystalline saturation solubility of NVP when in solution. Coformers that did not indicate potential interactions and miscibility with NVP were not considered for subsequent tests.

The formation of a stable CAM depends on the resulting interactions between its components, especially hydrogen bonds [50]. Molecular regions of 3TC and CAc can interact with NVP, forming two complex structures from the simultaneous interaction of its carbonyls and hydroxyls present in their molecules, with the carbonyl and amino group of NVP, resulting in greater stability to the formed system. The complexes NVP-3TC are formed through the interaction of NVP with 3TC in equivalent molar amounts. In the formation of hydrogen complexes, due to a redistribution in molecular electron density, the charge transfer involved in the donor–acceptor interaction should undoubtedly be considered [51]. In hydrogen interactions, charge transfer occurs from the lone pair of electrons of the proton acceptor atom to the antibonding orbital of the hydrogen bond, which results in bond stretching [52]. Due to the increase in the length of the hydrogen bond, there is a decrease in the vibration frequency when it establishes contact with the atom of the acceptor group [52, 53]. This phenomenon can occur in hydrogen interactions between NVP and its coformers, giving evidence of the formation of a CAM [53]. In fact, this was what occurred in all the hydrogen bonds of the complexes formed between NVP–3TC and NVP–CAc, which underwent an increase in their lengths and shifts to lower

frequencies were observed, indicating the possibility of hydrogen interactions between NVP and these compounds, also observed in the theoretical infrared spectrophotometric analysis.

A computational approach has already been used to verify the formation of amorphous formulations. Interactions between carbamazepine and α-Glycosyl rutine were analyzed through molecular dynamics simulation, mimicking the melt-quenching method, in addition to calculations by the orbital molecular fragment method. The authors realized that the multiple hydrogen interactions were greater than the interaction energy of the type π realized between drug and coformer [54]. Ceritinib CAMs were also obtained by a computational approach that estimated the binding energy and intermolecular interactions between the drug and different coformers to choose the best among them to stabilize the amorphous form of ceritinib [55]. Both works highlight the importance of the computational approach to obtain amorphous systems, especially because it provides information about different interactions that are difficult to detect by experimental approaches.

Although URE presents electronegative atoms in the molecule, such as oxygen and nitrogen in the carboxyl and amine groups which allow a great capacity for forming hydrogen bonds, the formation of NVP complex networks with URE molecules was not possible to occur. The URE crystalline structure is composed of eight hydrogen bonds distributed between six neighboring molecules, forming an infinite planar ribbon, with the carbonyl oxygen, accepting four hydrogen bonds instead of the two usually expected, promoting additional stabilization through forces dipole–dipole [56]. These stable interactions between URE molecules prevent the formation of new hydrogen bonds, and thus, the complex cannot be observed [57]. The crystalline form of the molecule and, consequently, its physical properties, such as conductivity, thermal stability, mechanical strength, and optical properties are influenced by hydrogen bonds, which acts as a vector of structural stability [58]. This characteristic makes the interaction between urea molecules highly stable, which favors the formation of their own networks, reducing the possibility of forming complexes with NVP or other molecules.

DSC is an instrumental technique widely used for rapid compatibility screening of different compounds and for producing amorphous samples from crystalline materials [30, 59]. The objective of the first heating carried out in the study was the melting of the physical mixtures with NVP and consequently their amorphization, while the DSC curves generated in the second heating characterize the material formed after the first heating, providing information about its homogeneity, miscibility of components, and evidence of crystalline material [60]. The crystalline nature of NVP was confirmed on the second heating, due to the recrystallization phenomenon that the drug underwent during the reheating process. The shift of the NVP melting point at PMs with 3TC and CAc suggests probable miscibility between the components, suggesting the possibility of formation of the amorphous systems, which did not occur with the mixture with URE, where the crystalline nature of NVP was evidenced and there was not good miscibility between the components [61].

When a material vitrifies when cooled from its melted state, it possesses the glass-forming ability, a method that classifies compounds into up to three classes. The first of these classes is defined when a material crystallizes during cooling, the second class is defined when crystallization occurs during reheating, while in the third class there is no crystallization [62]. Although the physical mixtures of NVP with 3TC and CAc indicate that there was miscibility between the components involved, it is perceived that the crystalline signal referring to NVP may indicate that it is not a complete miscibility and that these systems formed, together with the physical mixture with URE, are class II. Despite this, these results corroborate molecular studies, suggesting a better formation of amorphous systems of NVP with 3TC and CAc, through the possible intermolecular interactions that can be formed between them, while NVP and URE have difficulties in establishing bonds, making the formation of amorphous systems improbable.

The saturation solubility of NVP was investigated in its isolated crystalline form and in the presence of the coformers used in this study to verify their influence on its saturation crystalline solubility (Cs). In a review proposed by Korhonen and colleagues, it is asserted that the miscibility between the components is a significant parameter in the selection of excipients for co-amorphous formulations. It is proposed that the tendency of a stabilized amorphous drug to crystallize can be significantly influenced by the degree of mixing behavior between the drug and the coformer. Therefore, solubility parameters can be employed as a means of estimating the degree of molecular similarity [27].

NVP is a weak base with pKa equal to 2.8 and when present in aqueous media with a pH higher than 3, there are more non-ionized NVP molecules, lowering its solubility, and impairing its dissolution in the medium in question [63]. CAc is a carboxylic acid that contains -COOH and -OH groups that can interact with the drug through intermolecular interactions, such as ionic interactions and hydrogen bonds, with drugs with low aqueous solubility and weak bases such as NVP, forming salts of the drug, solubilizing it in the medium [64, 65]. A similar phenomenon could be observed in a study carried out with CAM with the weak base drug posaconazole, which showed increases in drug concentrations due to the acidic environment caused by CAc [66]. URE is a hydrotropic substance with an amphiphilic structure that forms free aggregates with drug molecules,

responsible for increasing the aqueous solubility of low-solubility drugs, especially when they are in non-ionized form [67].

In XRD analysis, PM can present the sum of the peaks of the individual components, a fact that occurred in all PMs obtained, where their diffraction angles showed the presence of crystalline NVP and the coformer used in all PMs. The presence of diffraction halos and the absence of peaks in CAMs confirms the amorphous nature of the material [68]. However, CAM 3TC shows signs of crystallinity that can lead to lower physical stability, but without recrystallization. CAMs of posaconazole obtained similar results for XRD analyses, but they were more stable in relation to solid dispersions of the same drug with the polymer Kollidon VA-64 which, due to the hygroscopicity of the system, absorbed moisture from the environment leading to recrystallization, which is more difficult to occur in CAM systems [66].

FTIR spectra obtained can reveal valuable information about the physical and chemical states of solid materials, especially when there is a change from the crystalline to the amorphous state, which can be related to shifting in bands in specific regions of the spectrum [30]. The NVP crystal is characterized by an amide function in a seven-membered ring, adopting a planar conformation, and there is also a cyclopropyl substituent [69, 70]. The changes perceived in the infrared spectra of CAMs corroborate the theoretical infrared studied in the screening. Such changes in the peak position and shape may be due to disruption of the structured crystal lattice into the amorphous state, suggesting that there were intermolecular interactions between NVP and its coformers, as occurred in nifedipine and ketoconazole CAMs, whose band shifts of groups involved in hydrogen bonds indicated interactions between the two compounds [71].

Intermolecular interactions play a key role in the stability of the amorphous drug forms and, consequently, a good CAM formation especially when these substances have at least two hydrogen donor/acceptor points, as is the case of the chosen components to stabilize the amorphous NVP [20]. Moreover, the amorphization of the material can also be suggested by the broadenings observed in the CAM spectra in the region between 3500 and 3000 cm^{-1} related to hydrogen bonds (Fig. 7b). The same phenomenon was observed with Atorvastatin-Irbesartan CAM, in which band shifts and broadenings were identified, suggesting that hydrogen interactions between the two drugs occurred, presenting co-amorphization [34]. The results observed through FTIR agree with those suggested in the screening tests, attesting that previous DSC and computational studies were relevant for the choice of coformers.

DSC assays indicated the recrystallization of the two drugs in PM 3TC, while partial miscibility between the components was shown in CAM 3TC. The intimate contact promoted by the preparation of the material may have caused interactions between the components since the preparation of the PMs and became more intense during the CAM formation process [20]. However, the thermal events found in CAM 3TC indicate that the amorphous material underwent recrystallization during the heating process, due to the NVP recrystallization and fusion processes. This recrystallization may have occurred due to the amount of crystalline material present in the CAM, whose crystalline nuclei may have received energy in the heating of the DSC and recrystallized.

The endothermic melting peaks of NVP in systems with CAc are displaced and at a lower intensity, showing that there may be a certain miscibility between the components, as verified in FTIR [61]. However, the results corroborate with XRD, which shows amorphization of the CAM CAc, but the material could have received energy to recrystallize as occurred in the CAM 3TC. Recrystallization events followed by drug fusion are possible to occur in co-amorphous materials, as in the case of indomethacin and tryptophan CAM, where peak exothermic recrystallization was followed by drug fusion [72]. The material was considered amorphous according to the authors' studies, but because they recrystallized at elevated temperatures, they were considered stable in relation to the isolated drug [72]. Besides, the reduction and shifting of the endothermic peaks of NVP in the presence of its coformers suggest partial miscibility of the compounds, through a possible partial dissolution of NVP with its fused coformers, as well as in the CAM formed between simvastatin and glipizide, which did not show intermolecular interactions, despite the formation of the amorphous system through a molecular mixture between the drugs, where glipizide served as a stabilizing agent of the amorphous form of simvastatin (anti-plasticizer) [73]. All The characterization results confirm the successful formation of CAMs, since there are differences between CAMs and PMs obtained, where the PLM photographs indicate numerous crystalline points referring to the starting materials in the PMs and that are not observed in the CAM slides.

It is common to observe improved dissolution rates of CAM obtained with two different drugs, compared to their isolated crystalline counterparts, as occurred with the CAM system of naproxen and cimetidine [74], whose dissolution rate was twice higher, without any evidence of crystallinity, due to the interactions between the two drugs in the exact proportion. The molecular proportion plays a fundamental role in the stability of CAM. The ratio 1:1 ratio is the most common and recommended, even though it is not mandatory, due to the number of specific intermolecular interactions between the components [74, 75]. Through these interactions, the compounds form heterodimers that remain formed when in contact with water, preventing recrystallization, which is possible to happen to pure components when they are in CAM of other molar proportions (Jensen *et al.* [76]). This indicates how the proportion between substances

in a CAM system is important for the dissolution of the drug and its increase in solubility.

The presence of CAc is responsible for the increase in the solubility of NVP, verified in the solubility tests, and the improvement is more evident in CAM in relation to its PM. This phenomenon can be explained by the maintenance of the amorphous structure stabilized by the intermolecular interactions between CAc and NVP generated during the formation of the complex, as observed in the characterizations and molecular dynamics [77]. Such interactions may have avoided the occurrence of nucleation and crystalline growth, preventing NVP recrystallization, as occurred in the CAM of loratadine and citric acid 1:1, whose dissolution revealed a solubility increase 50 times greater in relation to the isolated crystalline drug and up to 30 times greater in relation to it amorphous isolated [78].

CAMs can enhance the apparent final solubility of low-solubility drugs in a manner that is dependent on the specific interactions between the drug and its coformer. These interactions can facilitate an anti-plasticization effect within the system, thereby reducing molecular mobility. Additionally, the high energy inherent to the amorphous state and the absence of the energy required to rearrange the crystal structure during dissolution can be leveraged to further optimize the solubility of low-solubility drugs [23]. Moreover, improved wettability of the drug particles can significantly increase the dissolution rate, as it facilitates better interaction between the drug and the dissolution medium. The combined impact of these factors results in an enhanced solubility profile when compared to their crystalline counterparts and individual amorphous forms [20].

Considering the HIV treatment, the use of technologies that allow the improvement of drug solubility may play an important role in the HAART, as most drugs used in antiretroviral have first-pass metabolism, degradation in the gastrointestinal tract and low aqueous solubility, which leads to a short half-life, reduced and inconsistent bioavailability and risk of multidrug resistance [79]. In this aspect, the development of CAM to increase NVP solubility would be advantageous, especially when combined with 3TC, since a fixed-dose combination therapy using NVP:3TC CAM could not only overcome issues related to NVP solubility, but also make the therapy more accessible, reducing costs, and thus increasing patient treatment compliance.

Conclusion

The combined use of screening studies, namely computational, thermal, and solubility studies, was useful in developing NVP CAM. With these studies, it was possible to predict the formation of stable NVP CAM, by observing possible intermolecular interactions and a certain miscibility between the components. Computational methods were able to predict the formation of hydrogen complexes between NVP, 3TC and CAc. For all bonds involving hydrogen in the formation of complexes, shifts to lower frequencies occur, as well as an increase in these bonds CAM of NVP with 3TC and CAc was obtained through quench-cooling after the prediction of hydrogen interactions between the two components. When obtained, the NVP CAMs corroborated the screening studies, showing miscibility between the components, suggesting the formation of hydrogen interactions between NVP and its coformers, allowing the formation of the amorphous system verified by microscopy and XRD analysis. The maintenance of the amorphous form of NVP in CAM was also responsible for increasing the dissolution rate of NVP, reaching higher levels than the isolated drug and making CAM systems promising for antiretroviral combination therapy to combat HIV.

Supplementary Information The online version contains supplementary material available at https://doi.org/10.1208/s12249-024-02932-5.

Acknowledgements The authors would like to thank the *Coordination of Improvement of Higher Education Personnel* (CAPES) for the PhD fellowship; the authors thank *Pharmaceutical Laboratory in Pernambuco* (LAFEPE), *Drug Technology Laboratory* (LTM) of the Federal University of Pernambuco and *Laboratory of Technology of Nanosystems Carriers of Active Substances—TecNano* for solid state characterizations.

Author Contributions KAS: research idea conceptualization, conducted laboratory work, conducted data analysis, manuscript writing; and editing. LLC: data analysis, revised and edited the manuscript. DN: conducted laboratory work, conducted data analysis. MFLR: research idea conceptualization, manuscript revision, and study supervision. JLSS: research idea conceptualization, supervised the study, data analysis, revised and edited the manuscript. All authors read and approved the final manuscript.

Funding This work was supported by the FINEP-FADE-UFPE under Grant 0120–21.

Data Availability The records generated and investigated during the study are available from the corresponding author on demand.

Declarations

Conflict of Interest The authors declare that they have no known competing financial interests or personal relationships that could have appeared to influence the work reported in this paper.

References

1. World Health Organization. HIV and AIDS [Internet]. 2023 [cited 2023 Sep 18]. Available from: https://www.who.int/news-room/fact-sheets/detail/hiv-aids
2. Arca HÇ, Mosquera-Giraldo LI, Dahal D, Taylor LS, Edgar KJ. Multidrug, Anti-HIV Amorphous Solid Dispersions: Nature and

Mechanisms of Impacts of Drugs on Each Other's Solution Concentrations. Mol Pharm. 2017;14:3617–27.
3. Santos KA dos, Danda LJ de A, Oliveira TC de, Soares-Sobrinho JL, Soares MF de LR. The drug loading impact on dissolution and diffusion: a case-study with amorphous solid dispersions of nevirapine. Research, Society and Development. 2022;11:e168111436117.
4. Panzade P, Somani P, Rathi P. Nevirapine Pharmaceutical Cocrystal: Design. Development and Formulation Drug Deliv Lett. 2019;9:240–7.
5. Rao MRP, Sonawane AS, Sapate SA, Mehta CH, Nayak UY. Molecular modeling and in vitro studies to assess solubility enhancement of nevirapine by solid dispersion technique. J Mol Struct. 2023;1273: 134373.
6. Tambosi G, Coelho PF, Soares L, Lenschow ICS, Zétola M, Stulzer HK, *et al*. Challenges to improve the biopharmaceutical properties of poorly water-soluble drugs and the application of the solid dispersion technology. Revista Materia. 2018;23:e12224.
7. Savjani KT, Gajjar AK, Savjani JK. Drug Solubility: Importance and Enhancement Techniques. ISRN Pharm [Internet]. 2012;2012:1–10. Available from: https://www.hindawi.com/archive/2012/195727/
8. Blaabjerg LI, Bulduk B, Lindenberg E, Löbmann K, Rades T, Grohganz H. Influence of Glass Forming Ability on the Physical Stability of Supersaturated Amorphous Solid Dispersions. J Pharm Sci. 2019;108:2561–9.
9. Cooper ER. Nanoparticles: A personal experience for formulating poorly water soluble drugs. J Control Release. 2010;141:300–2.
10. Shegokar R, Singh KK. Surface modified nevirapine nanosuspensions for viral reservoir targeting: In vitro and in vivo evaluation. Int J Pharm. 2011;421:341–52.
11. Zhu Y, Ye J, Zhang Q. Self-emulsifying Drug Delivery System Improve Oral Bioavailability: Role of Excipients and Physicochemical Characterization. Pharm Nanotechnol. 2020;8:290–301.
12. Tang J, Sun J, He Z-G. Self-Emulsifying Drug Delivery Systems: Strategy for Improving Oral Delivery of Poorly Soluble Drugs. Curr Drug ther. 2008;2:85–93.
13. Singh G, Singh N, Kumar R, Bedi N. Development and characterization of nevirapine loaded amorphous solid dispersions for solubility enhancement. Asian J Pharm Clin Res. 2019;12:176–82.
14. Ivone R, Fernando A, DeBoef B, Meenach SA, Shen J. Development of Spray-Dried Cyclodextrin-Based Pediatric Anti-HIV Formulations. AAPS PharmSciTech. 2021;22:193.
15. Hiew TN, Zemlyanov DY, Taylor LS. Balancing Solid-State Stability and Dissolution Performance of Lumefantrine Amorphous Solid Dispersions: The Role of Polymer Choice and Drug-Polymer Interactions. Mol Pharm. 2022;19:392–413.
16. Fong SYK, Bauer-Brandl A, Brandl M. Oral bioavailability enhancement through supersaturation: an update and meta-analysis. Expert Opin Drug Deliv. 2017;14:403–26.
17. Laitinen R, Löbmann K, Grohganz H, Priemel P, Strachan CJ, Rades T. Supersaturating drug delivery systems: The potential of co-amorphous drug formulations. Int J Pharm. 2017;532:1–12.
18. Sarode AL, Wang P, Obara S, Worthen DR. Supersaturation, nucleation, and crystal growth during single- and biphasic dissolution of amorphous solid dispersions: Polymer effects and implications for oral bioavailability enhancement of poorly water soluble drugs. Eur J Pharm Biopharm. 2014;86:351–60.
19. Baghel S, Cathcart H, O'Reilly NJ. Polymeric Amorphous Solid Dispersions: A Review of Amorphization, Crystallization, Stabilization, Solid-State Characterization, and Aqueous Solubilization of Biopharmaceutical Classification System Class II Drugs. J Pharm Sci. 2016;105:2527–44.
20. Karagianni A, Kachrimanis K, Nikolakakis I. Co-Amorphous Solid Dispersions for Solubility and Absorption Improvement of Drugs: Composition, Preparation, Characterization and Formulations for Oral Delivery. Pharmaceutics. 2018;10:1–26.
21. Mizoguchi R, Waraya H, Hirakura Y. Application of Co-Amorphous Technology for Improving the Physicochemical Properties of Amorphous Formulations. Mol Pharm. 2019;16:2142–52.
22. Yarlagadda DL, Sai Krishna Anand V, Nair AR, Navya Sree KS, Dengale SJ, Bhat K. Considerations for the selection of co-formers in the preparation of co-amorphous formulations. Int J Pharm. 2021 602:120649.
23. Vullendula SKA, Nair AR, Yarlagadda DL, Navya Sree KS, Bhat K, Dengale SJ. Polymeric solid dispersion Vs co-amorphous technology: A critical comparison. J Drug Deliv Sci Technol. 2022;78: 103980.
24. Han J, Wei Y, Lu Y, Wang R, Zhang J, Gao Y, *et al*. Co-amorphous systems for the delivery of poorly water-soluble drugs: recent advances and an update. Expert Opin Drug Deliv. 2020;17:1411–35.
25. Liu J, Grohganz H, Löbmann K, Rades T, Hempel NJ. Co-amorphous drug formulations in numbers: Recent advances in co-amorphous drug formulations with focus on co-formability, molar ratio, preparation methods, physical stability, *in vitro* and *in vivo* performance, and new formulation strategies. Pharmaceutics. 2021;13:389.
26. Shi X, Zhou X, Shen S, Chen Q, Song S, Gu C, *et al*. Improved *in vitro* and *in vivo* properties of telmisartan in the co-amorphous system with hydrochlorothiazide: A potential drug-drug interaction mechanism prediction. Eur J Pharm Sci. 2021;161:105773.
27. Korhonen O, Pajula K, Laitinen R. Rational excipient selection for co-amorphous formulations. Expert Opin Drug Deliv. 2016;14:551–69.
28. Dennington R, Keith T, Millam J. Gauss View. Shawnee Mission: Semichem Inc.; 2009.
29. Froese FC. General Hartree-Fock program. Comput Phys Commun. 1987;43:355–65.
30. D'Angelo A, Edgar B, Hurt AP, Antonijević MD. Physico-chemical characterisation of three-component co-amorphous systems generated by a melt-quench method. J Therm Anal Calorim. 2018;134:381–90.
31. Chadha R, Arora P, Garg M, Bhandari S, Jain DS. Thermoanalytical and spectroscopic studies on different crystal forms of nevirapine. J Therm Anal Calorim. 2013;111:2133–42.
32. Food and Drug Administration. FDA. Waiver of *in vivo* bioavailability and bioequivalence studies for immediate-release solid dosage forms base on a Biopharmaceutics Classification System. Maryland; 2017. p. 1–19.
33. Baka E, Comer JEA, Takács-Novák K. Study of equilibrium solubility measurement by saturation shake-flask method using hydrochlorothiazide as model compound. J Pharm Biomed Anal. 2008;46:335–41.
34. Skotnicki M, Jadach B, Skotnicka A, Milanowski B, Tajber L, Pyda M, *et al*. Physicochemical characterization of a co-amorphous atorvastatin-irbesartan system with a potential application in fixed-dose combination therapy. Pharmaceutics. 2021;13:1–20.
35. Vieira-Sellaï L, Quintana M, Diop O, Mercier O, Tarrit S, Raimi N, *et al*. Green HPLC quantification method of lamivudine, zidovudine and nevirapine with identification of related substances in tablets. Green Chem Lett Rev. 2022;15:695–704.
36. Anbazhagan S, Indumathy N, Shanmugapandiyan P, Sridhar SK. Simultaneous quantification of stavudine, lamivudine and nevirapine by UV spectroscopy, reverse phase HPLC and HPTLC in tablets. J Pharm Biomed Anal. 2005;39:801–4.
37. Lodagekar A, Chavan RB, Mannava MKC, Yadav B, Chella N, Nangia AK, *et al*. Co amorphous valsartan nifedipine system:

Preparation, characterization, *in vitro* and *in vivo* evaluation. Eur J Pharm Sci. 2019;139: 105048.
38. Zhang Y, Huo M, Zhou J, Zou A, Li W, Yao C, *et al*. DDSolver: An add-in program for modeling and comparison of drug dissolution profiles. AAPS J. 2010;12:263–71.
39. Porfírio LDO, Costa AA, Conceição RR, Matos TDO, Almeida EDP, Sarmento VHV, *et al*. Compatibility study of hydroxypropylmethylcellulose films containing zidovudine and lamivudine using thermal analysis and infrared spectroscopy. J Therm Anal Calorim. 2015;120:817–28.
40. Reguri BR, Chakka R. Crystalline forms of nevirapine. Estados Unidos; 2006. p. 1–7.
41. Sarkar M, Perumal OP, Panchagnula R. Solid-state characterization of nevirapine. Indian J Pharm Sci. 2008;70:619–30.
42. Palei NN, Mamidi SK, Rajangam J. Formulation and evaluation of lamivudine sustained release tablet using okra mucilage. J Appl Pharm Sci. 2016;6:069–75.
43. Baruah U, Deka MJ, Chowdhury D. Reversible on/off switching of fluorescence via esterification of carbon dots. RSC Adv. 2014;4:36917–22.
44. Pimpang P, Sumang R, Choopun S. Effect of concentration of citric acid on size and optical properties of fluorescence graphene quantum dots prepared by tuning carbonization degree. Chiang Mai J Sci. 2018;45:2005–14.
45. Hirakawa Y, Ueda H, Miyano T, Kamiya N, Goto M. New insight into transdermal drug delivery with supersaturated formulation based on co-amorphous system. Int J Pharm. 2019;569:118582.
46. Chambers LI, Musa OM, Steed JW. Prediction and Preparation of Coamorphous Phases of a Bislactam. Mol Pharm. 2022;19:2651–61.
47. Ahuja N, Katare OP, Singh B. Studies on dissolution enhancement and mathematical modeling of drug release of a poorly water-soluble drug using water-soluble carriers. Eur J Pharm Biopharm. 2007;65:26–38.
48. Hirakawa Y, Ueda H, Takata Y, Minamihata K, Wakabayashi R, Kamiya N, *et al*. Co-amorphous formation of piroxicam-citric acid to generate supersaturation and improve skin permeation. Eur J Pharm Sci. 2021;158:105667.
49. Ueda H, Wu W, Löbmann K, Grohganz H, Müllertz A, Rades T. Application of a Salt Coformer in a Co-Amorphous Drug System Dramatically Enhances the Glass Transition Temperature: A Case Study of the Ternary System Carbamazepine, Citric Acid, and l -Arginine. Mol Pharm. 2018;15:2036–44.
50. Deng Y, Liu S, Jiang Y, Martins ICB, Rades T. Recent Advances in Co-Former Screening and Formation Prediction of Multicomponent Solid Forms of Low Molecular Weight Drugs. Pharmaceutics. 2023;15:2174.
51. Zhang Z, Li D, Jiang W, Wang Z. The electron density delocalization of hydrogen bond systems. Adv Phys X. 2018;3:1428915.
52. Takahashi M, Okamura N, Ding X, Shirakawa H, Minamide H. Intermolecular hydrogen bond stretching vibrations observed in terahertz spectra of crystalline vitamins. CrystEngComm. 2018;20:1960–9.
53. Kolesov B. Hydrogen Bonds: Raman Spectroscopic Study. Int J Mol Sci. 2021;22:5380.
54. Ma X, Higashi K, Fukuzawa K, Ueda K, Kadota K, Tozuka Y, *et al*. Computational approach to elucidate the formation and stabilization mechanism of amorphous formulation using molecular dynamics simulation and fragment molecular orbital calculation. Int J Pharm. 2022;615: 121477.
55. Yarlagadda DL, Anand VSK, Nair AR, Dengale SJ, Pandiyan S, Mehta CH, *et al*. A computational-based approach to fabricate Ceritinib co-amorphous system using a novel co-former Rutin for bioavailability enhancement. Eur J Pharm Biopharm. 2023;190:220–30.
56. Ferrero M, Civalleri B, Rérat M, Orlando R, Dovesi R. The calculation of the static first and second susceptibilities of crystalline urea: A comparison of Hartree–Fock and density functional theory results obtained with the periodic coupled perturbed Hartree–Fock/Kohn–Sham scheme. J Chem Phys. 2009;131.
57. Civalleri B, Doll K, Zicovich-Wilson CM. Ab initio investigation of structure and cohesive energy of crystalline urea. J Phys Chem B. 2007;111:26–33.
58. Perpétuo GJ, Janczak J. Supramolecular hydrogen-bonding networks in the 1-(diaminomethylenene) thiouron-1-ium 4-hydroxybenzoate, 3,4-dihydroxybenzoate and 3,4,5- trihydroxybenzoate monohydrate crystals. J Mol Struct. 2013;1041:127–38.
59. Maheswaram MP, Mantheni D, Perera I, Venumuddala H, Riga A, Alexander K. Characterization of crystalline and amorphous content in pharmaceutical solids by dielectric thermal analysis. J Therm Anal Calorim. 2013;111:1987–97.
60. Rojek B, Wesolowski M. A combined differential scanning calorimetry and thermogravimetry approach for the effective assessment of drug substance-excipient compatibility. J Therm Anal Calorim. 2023;148:845–58.
61. Datta A, Nolas GS. Composition controlled synthesis of Bi rich Bi1−xSbx alloy nanocrystals by a low temperature polyol process. CrystEngComm. 2011;13:2753.
62. Alhalaweh A, Alzghoul A, Kaialy W, Mahlin D, Bergström CAS. Computational Predictions of Glass-Forming Ability and Crystallization Tendency of Drug Molecules. Mol Pharm [Internet]. 2014 [cited 2022 Feb 15];11:3123–32. Available from: https://pubs.acs.org/doi/full/10.1021/mp500303a
63. Adeola AO, de Lange J, Forbes PBC. Adsorption of antiretroviral drugs, efavirenz and nevirapine from aqueous solution by graphene wool: Kinetic, equilibrium, thermodynamic and computational studies. Appl Surf Sci Adv. 2021;6: 100157.
64. Nangare S, Vispute Y, Tade R, Dugam S, Patil P. Pharmaceutical applications of citric acid. Futur J Pharm Sci. 2021;7:1–23.
65. Wu W, Ueda H, Löbmann K, Rades T, Grohganz H. Organic acids as co-formers for co-amorphous systems – Influence of variation in molar ratio on the physicochemical properties of the co-amorphous systems. Eur J Pharm Biopharm. 2018;131:25–32.
66. Wu H, Ma J, Qian S, Jiang W, Liu Y, Li J, *et al*. Co-amorphization of posaconazole using citric acid as an acidifier and a co-former for solubility improvement. J Drug Deliv Sci Technol. 2023;80: 104136.
67. Beig A, Lindley D, Miller JM, Agbaria R, Dahan A. Hydrotropic solubilization of lipophilic drugs for oral delivery: The effects of urea and nicotinamide on carbamazepine solubility-permeability interplay. Front Pharmacol. 2016;7:379.
68. Krstić M, Manić L, Martić N, Vasiljević D, Mračević SĐ, Vukmirović S, *et al*. Binary polymeric amorphous carvedilol solid dispersions: *In vitro* and *in vivo* characterization. Eur J Pharm Sci. 2020;150: 105343.
69. Mui PW, Jacober SP, Hargrave KD, Adams J. Crystal structure of nevirapine, a non-nucleoside inhibitor of HIV-1 reverse transcriptase, and computational alignment with a structurally diverse inhibitor. J Med Chem. 1992;35:201–2.
70. Ayala AP, Siesler HW, Wardell SMSV, Boechat N, Dabbene V, Cuffini SL. Vibrational spectra and quantum mechanical calculations of antiretroviral drugs: Nevirapine. J Mol Struct. 2007;828:201–10.
71. Hatanaka Y, Uchiyama H, Kadota K, Tozuka Y. Improved solubility and permeability of both nifedipine and ketoconazole

based on coamorphous formation with simultaneous dissolution behavior. J Drug Deliv Sci Technol. 2021;65: 102715.
72. Jensen KT, Larsen FH, Cornett C, Löbmann K, Grohganz H, Rades T. Formation Mechanism of Coamorphous Drug-Amino Acid Mixtures. Mol Pharm. 2015;12:2484–92.
73. Löbmann K, Strachan C, Grohganz H, Rades T, Korhonen O, Laitinen R. Co-amorphous simvastatin and glipizide combinations show improved physical stability without evidence of intermolecular interactions. Eur J Pharm Biopharm. 2012;81:159–69.
74. Allesø M, Chieng N, Rehder S, Rantanen J, Rades T, Aaltonen J. Enhanced dissolution rate and synchronized release of drugs in binary systems through formulation: Amorphous naproxen–cimetidine mixtures prepared by mechanical activation. J Control Release. 2009;136:45–53.
75. Löbmann K, Laitinen R, Grohganz H, Gordon KC, Strachan C, Rades T. Coamorphous drug systems: enhanced physical stability and dissolution rate of indomethacin and naproxen. Mol Pharm. 2011;8:1919–28.
76. Jensen KT, Larsen FH, Löbmann K, Rades T, Grohganz H. Influence of variation in molar ratio on co-amorphous drug-amino acid systems. Eur J Pharm Biopharm. 2016;107:32–9.
77. Lambros M, Tran T, Fei Q, Nicolaou M. Citric Acid: A Multifunctional Pharmaceutical Excipient. Pharmaceutics. 2022;14:972.
78. Wang J, Chang R, Zhao Y, Zhang J, Zhang T, Fu Q, *et al*. Coamorphous Loratadine-Citric Acid System with Enhanced Physical Stability and Bioavailability. AAPS PharmSciTech. 2017;18:2541–50.
79. Hari BV, Devendharan K, Narayanan N. Approaches of Novel drug delivery systems for Anti-HIV agents. Int J Drug Dev Res. 2013;5:1–9.